Size effects in epitaxial ferroelectric islands and thin films

Jie Wang and Tong-Yi Zhang*
Department of Mechanical Engineering, Hong Kong University of Science and Technology, Clear Water Bay, Kowloon, Hong Kong, China

(Received 7 January 2006; revised manuscript received 27 February 2006; published 13 April 2006)

Size effects on domain configuration and polarization switching in two-dimensional epitaxial ferroelectric islands and in thin films are investigated by using a continuum phase field model that incorporates long-range elastic and electrostatic interactions. The simulations exhibit spatial polarization distributions with different types of domain walls in the epitaxial ferroelectric islands and find two critical thicknesses, at which the simulated material changes from a multidomain state to a single-domain state and from ferroelectric phase to paraelectric phase, respectively. The two critical thicknesses and the domain wall types vary with the length-to-thickness ratio. The simulations show that macroscopic polarization switching in thin films under an external electric field is processed through the nucleation of new domains and domain wall motion. The remanent polarization and the coercive field of the simulated ferroelectric films both decrease with decreasing film thickness.

DOI: 10.1103/PhysRevB.73.144107 PACS number(s): 77.80.Dj, 77.84.Dy, 77.80.Fm, 77.80.Bh

I. INTRODUCTION

Currently, material properties of ferroelectric epitaxial islands and thin films at the nanometer scale receive considerable attention from academics and industries due to the potential integration of nanoferroelectrics into microelectronics.[1–3] Ferroelectric properties substantially deviate from the bulk behavior as the particle size or the film thickness is reduced to nanometers. For example,[4,5] a $PbTiO_3$ particle is a single domain when its diameter is less than 20 nm and the ferroelectricity may eventually disappear when the diameter is below 4.2 nm. Obviously, to understand the size-dependent behavior of ferroelectrics is academically significant and practically important. Therefore, different theoretical approaches, including phenomenological Landau theories and atomic-level first-principles calculations, have been used to study the size-dependent ferroelectric properties in quantum dots,[6] thin films,[7,8] nanodisks, and nanorods.[9] First-principles calculations have greatly contributed to the understanding of the origin of ferroelectric structures and properties and to mechanisms of ferroelectric instabilities.[10] Based on first-principles calculations, Junuera and Ghosez[8] showed that a $BaTiO_3$ film between two metallic $SrRuO_3$ electrodes in short circuit lost the ferroelectric properties when its thickness was thinner than a critical thickness of about six unit cells ($\sim$2.4 nm). Recently, Fu *et al.* used a first-principles-derived effective Hamiltonian approach to study the size-dependent properties in ferroelectric nanodisks and nanorods and found an unusual phase transition.[9] To account for the surface effect, the interaction between the local modes at surface and the vacuum, and the interaction between the inhomogeneous strains and the vacuum are added into the Hamiltonian.

In addition to the first-principles calculations, continuum theories may be also powerful in studying ferroelectric particles and films at the nanoscale.[2] For example, one-dimensional Landau-Ginzburg theories have successfully explored the critical size for polarization instability in stress-free ferroelectric particles and in ferroelectric thin films.[5,11,12] In the study of nanoferroelectrics by continuum theories, appropriate boundary conditions must be applied along surfaces of a finite-size particle. The boundary condition for polarization, $\mathbf{P}$, is usually given by $d\mathbf{P}/dn=-\mathbf{P}/\delta$,[5,11,12] where n refers to a unit length in the outward normal direction of the surface and δ is the so-called extrapolation length, which is introduced to describe the difference in polarizations between the surface and the interior of the material. The polarization is reduced at the surface when δ is positive or zero, while the polarization is enhanced at the surface when δ is negative. Therefore, the value of δ determines the intrinsic size effect. When δ approaches infinity, the boundary condition becomes $d\mathbf{P}/dn=0$, which is called the free boundary condition,[13] and the intrinsic size effect vanishes because in this case, there is no difference for polarizations in the media between the surface and the interior. When δ equals zero, polarizations are completely suppressed, i.e., $\mathbf{P}=0$, at the surface, which is called the zero boundary condition,[13] thereby generating the most significant size effect. The δ value should be determined by first-principles calculations and/or by carefully designed experiments, which will be the future task of research. Currently, various values of δ are approximately used in the literature for simplicity.

Phase field models of ferroelectrics are based on the Landau-Ginzburg theory and take the long-range electrostatic and elastic interactions into account.[14–16] To simplify numerical calculations, periodic boundary conditions are usually employed in phase field simulations of ferroelectrics[17–19] with the highly efficient fast Fourier transform technique such that elastic solution for a given polarization distribution can be obtained analytically in reciprocal space. However, periodic boundary conditions may be inappropriate in simulations of nanoferroelectrics because a nanoferroelectric material has a finite size and thus boundary conditions should, in general, not be periodic. Therefore, it is necessary for phase field simulations of nanoferroelectrics to develop novel simulation models and methods that allow direct applications of arbitrary mechanical and electrical

boundary conditions and make the computation size physically meaningful and practically implemental. By using the finite element method, Cao *et al.*[20] made such an effort to simulate domain formation in a finite ferroelectric system without taking periodic boundary conditions. In their simulations, however, the long-range electrostatic and elastic interactions were not taken into account.[20] Zhang and Bhattacharya[21] developed a computational model for ferroelectrics subjected to realistic electromechanical boundary conditions and studied the nucleation of domains and propagation of domain walls in thin films under combined electromechanical loading. In the present work, we consider the long-range electrostatic and elastic interactions without using periodic boundary conditions to simulate material behaviors and electrical domain structures of ferroelectric islands and thin films, which are grown on substrates, as shown in Figs. 1(a) and 1(b), respectively.

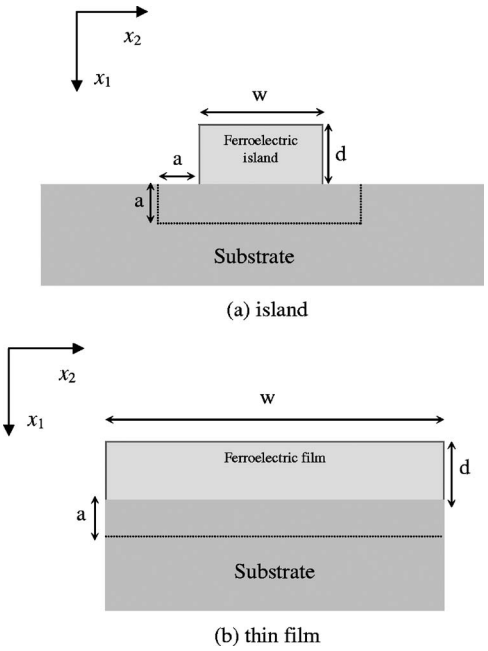

FIG. 1. Schematic diagram of a nanoscale ferroelectric (a) island or (b) thin film grown on a substrate, where "w" and "d" denote the length and the thickness, respectively. The elastic deformation of the substrate inside the area surrounded by dotted lines is calculated in the simulations and $a/d=0.6$.

II. SIMULATION METHODOLOGY

A. General approach of the phase field model for nanoferroelectrics

Spontaneous polarization occurs in a ferroelectric material when the temperature is lower than its Curie point, thereby leading to the paraelectric-to-ferroelectric phase transition. In the present phase field simulations, we may regard that spontaneous polarizations associated with spontaneous strains are embedded in a background material, i.e., in the paraelectric phase material. When an electric field, $\mathbf{E}$, is present, the electric field will induce a polarization field. Thus, the total polarization, $\mathbf{P}^{(t)}$, can be divided into two components, the spontaneous polarization, $\mathbf{P}$, and the induced polarization, $\mathbf{P}^{(i)}$. For simplicity, the induced polarization may be assumed to be linearly proportional to the electric field.[22] In this case, the electric displacement vector, $\mathbf{D}$, can be given by

$$\mathbf{D} = \varepsilon_0 \mathbf{E} + \mathbf{P}^{(t)} = \varepsilon_0 \mathbf{E} + \mathbf{P}^{(i)} + \mathbf{P} = \varepsilon_0 \boldsymbol{\kappa} \mathbf{E} + \mathbf{P}, \tag{1}$$

where $\varepsilon_0 = 8.85 \times 10^{-12}$ Fm^{-1} is the dielectric constant of the vacuum and $\boldsymbol{\kappa}$ denotes the relative dielectric constant tensor of the background material. Since the background material is the paraelectric phase, which has a cubic crystal structure, the relative dielectric constant matrix is diagonal and the relative dielectric constants in three axis directions are the same, i.e., $\kappa = \kappa_{11} = \kappa_{22} = \kappa_{33}$ and $\kappa_{ij} = 0 (i \neq j)$. The spontaneous polarization vector, $\mathbf{P} = (P_1, P_2, P_3)$, is usually used as the order parameter to calculate thermodynamic energies of the ferroelectric phase in the Laudau phase transformation theory. The standard Landau-Devonshire energy density is[23]

$$\begin{aligned} f_{LD}(P_i, \sigma_{ij}) = {} & \alpha_1 (P_1^2 + P_2^2 + P_3^2) + \alpha_{11} (P_1^4 + P_2^4 + P_3^4) + \alpha_{12} (P_1^2 P_2^2 + P_2^2 P_3^2 + P_1^2 P_3^2) + \alpha_{111} (P_1^6 + P_2^6 + P_3^6) + \alpha_{112} [(P_1^4 (P_2^2 + P_3^2) \\ & + P_2^4 (P_1^2 + P_3^2) + P_3^4 (P_1^2 + P_2^2)\ ] + \alpha_{123} P_1^2 P_2^2 P_3^2 - \tfrac{1}{2} s_{11} (\sigma_{11}^2 + \sigma_{22}^2 + \sigma_{33}^2) - s_{12} (\sigma_{11}\sigma_{22} + \sigma_{22}\sigma_{33} + \sigma_{11}\sigma_{33}) \\ & - \tfrac{1}{2} s_{44} (\sigma_{12}^2 + \sigma_{23}^2 + \sigma_{13}^2) - Q_{11} (\sigma_{11} P_1^2 + \sigma_{22} P_2^2 + \sigma_{33} P_3^2) - Q_{12} [\sigma_{11} (P_2^2 + P_3^2) + \sigma_{22} (P_1^2 + P_3^2) + \sigma_{33} (P_1^2 + P_2^2)] \\ & - Q_{44} (\sigma_{12} P_1 P_2 + \sigma_{13} P_1 P_3 + \sigma_{23} P_2 P_3), \end{aligned} \tag{2}$$

where $\alpha_1 = (T - T_0)/2\varepsilon_0 C_0$ is the dielectric stiffness, $\alpha_{11}, \alpha_{12}, \alpha_{111}, \alpha_{112}, \alpha_{123}$ are higher order dielectric stiffnesses, T and T_0 denote temperature and the Curie-Weiss temperature, respectively, C_0 is the Curie constant; s_{ij} are the elastic compliance coefficients, Q_{ij} are electrostrictive constants, and σ_{ij} denote mechanical stresses. Note that mechanical stresses include applied and internal stresses induced by spontaneous strains.

In the Ginzburg-Landau theory, the free energy function also depends on the gradient of the order parameter. For ferroelectric materials, the polarization gradient energy represents also the domain wall energy. For simplicity, the low-

est order of the gradient energy density is used here, which takes the form:

$$f_G(P_{i,j}) = \frac{1}{2}G_{11}(P_{1,1}^2 + P_{2,2}^2 + P_{3,3}^2) + G_{12}(P_{1,1}P_{2,2} + P_{2,2}P_{3,3} + P_{1,1}P_{3,3}) + \frac{1}{2}G_{44}[(P_{1,2} + P_{2,1})^2 + (P_{2,3} + P_{3,2})^2 + (P_{1,3} + P_{3,1})^2] + \frac{1}{2}G'_{44}[(P_{1,2} - P_{2,1})^2 + (P_{2,3} - P_{3,2})^2 + (P_{1,3} - P_{3,1})^2], \quad (3)$$

where G_{11}, G_{12}, G_{44}, and G'_{44} are gradient energy coefficients, and $P_{i,j}$ denotes the derivative of the ith component of the polarization vector, P_i, with respect to the jth coordinate and $i, j=1,2,3$.

To describe the finite-size ferroelectrics with multidomain structures, the total free energy should include depolarization energy induced by spatially inhomogeneous spontaneous polarizations. The depolarization field is a self-electrostatic field which is dependent on the spontaneous polarizations. The depolarization energy is a self-electrostatic energy corresponding to the long-range electrostatic interaction of spontaneous polarizations and is calculated by[22,24,25]

$$f_{dep} = -\tfrac{1}{2}(E_1^d P_1 + E_2^d P_2 + E_3^d P_3), \quad (4)$$

where E_1^d, E_2^d, and E_3^d are the components of the depolarization field along the x_1, x_2, and x_3 axes, respectively. The self-electrostatic field is the negative gradient of the electrostatic potential, ϕ, induced by spontaneous polarizations, i.e., $E_i^d = -\phi_{,i}$. The electrostatic potential can be obtained by solving the following electrostatic equilibrium equation:

$$\mathbf{D}_{i,i} = (\varepsilon_0 \boldsymbol{\kappa}\mathbf{E} + \mathbf{P})_{i,i} = 0, \text{ or} \quad (5a)$$

$$\varepsilon_0 \kappa(\phi_{,11} + \phi_{,22} + \phi_{,33}) = P_{1,1} + P_{2,2} + P_{3,3}, \quad (5b)$$

for a body-charge-free paraelectric medium.[11,22,25] Note that the dielectric constant, κ, in Eq. (5) denotes the relative dielectric constant of the background paraelectric material, which is a scale. The same homogeneous and isotropic assumption was used in Refs. 14 and 25. Equation (5) is solved by using the finite difference method for a given polarization distribution and predescribed boundary conditions. If an externally electric field, E_i^a, is applied to the system, the applied field generates an additional electrical energy density,

$$f_{elec} = -E_i^a P_i. \quad (6)$$

Integrating all free energy densities over the entire volume of a simulated ferroelectric material yields the total free energy, F, of the simulated ferroelectric material:

$$F = \int_V [f_{LD}(P_i, \sigma_{ij}) + f_G(P_{i,j}) + f_{dep}(P_i, E_i^d) + f_{elec}(P_i, E_i^a)]dV, \quad (7)$$

where V denotes the volume of the simulated ferroelectric material.

In phase-field simulations,[14–18] it is usually assumed that the mechanical and electric equilibrium be established instantaneously once a spontaneous polarization distribution is set down. If no external stresses and electric fields are applied to the system, inhomogeneously distributed polarizations induce an internal stress field, σ_{ij}, and a depolarization field, E_i^d. In this case, the total free energy is determined by the spontaneous polarization field.

The temporal evolution of the spontaneous polarization field is described by the time-dependent Ginzburg-Landau equation,

$$\frac{\partial P_i(\mathbf{r},t)}{\partial t} = -L\frac{\delta F}{\delta P_i(\mathbf{r},t)} \quad (i=1,2,3), \quad (8)$$

where L is the kinetic coefficient, $\delta F / \delta P_i(\mathbf{r},t)$ represents the thermodynamic driving force of the spatial and temporal evolution of the simulated system, $\mathbf{r}=(x_1,x_2,x_3)$ is the spatial vector, and t denotes time.

B. Dimensionless equations for a two-dimensional system with the zero surface spontaneous polarization

Two-dimensional (2D) simulations are conducted in the present work under the plane-stress condition along the x_3 axis, although the methodology described in Sec. II A can be applied to three-dimensional simulations. For a finite size 2D ferroelectric material coherently constrained by an elastic substrate, as shown in Fig. 1(a) or 1(b), we adopt the zero boundary condition for spontaneous polarizations for simplicity. This means that for a 2D island shown in Fig. 1(a), we set $P_1=0$ and $P_2=0$ along the three surfaces and the interface between the simulated ferroelectric material and the substrate. For a 2D thin film shown in Fig. 1(b), we set $P_1=0$ and $P_2=0$ at the top surface and the interface and use the periodic boundary condition in the x_2 direction. The zero boundary condition is obviously approximate, but it is simple, because the surface energy term vanishes, and it can explain some experimental observations.[26] The zero boundary condition has been used by other researchers in the simulations of 2D fully constrained ferroelectrics[16] and in the study of ferroelectric thin films.[13] Moreover, the spontaneous polarization component, P_3, and the electric field component, E_3, are treated as zeros in the present 2D simulations. For convenience, we employ the following set of the dimensionless variables for Eq. (8) (Ref. 14):

$$\mathbf{r}^* = \sqrt{|\alpha_0|/G_{110}}\mathbf{r}, \quad t^* = |\alpha_0|Lt, \quad \mathbf{P}^* = \mathbf{P}/P_0, \quad \varepsilon_0^* = \varepsilon_0|\alpha_0|$$

$$\alpha_1^* = \alpha_1/|\alpha_0|, \quad \alpha_{11}^* = \alpha_{11}P_0^2/|\alpha_0|, \quad \alpha_{12}^* = \alpha_{12}P_0^2/|\alpha_0|,$$

$$\alpha_{111}^* = \alpha_{111}P_0^4/|\alpha_0|, \quad \alpha_{112}^* = \alpha_{112}P_0^4/|\alpha_0|, \quad \alpha_{123}^* = \alpha_{123}P_0^4/|\alpha_0|,$$

$$Q_{11}^* = Q_{11}P_0^2, \quad Q_{12}^* = Q_{12}P_0^2, \quad Q_{44}^* = Q_{44}P_0^2,$$

$$s_{11}^* = s_{11}(|\alpha_0|P_0^2), \quad s_{12}^* = s_{12}(|\alpha_0|P_0^2), \quad s_{44}^* = s_{44}(|\alpha_0|P_0^2),$$

TABLE I. Values of the normalized coefficients used in the simulations.

α_{11}^*	α_{12}^*	α_{111}^*	α_{112}^*	α_{123}^*	Q_{11}^*	Q_{12}^*	Q_{44}^*	s_{11}^*	s_{12}^*	s_{44}^*	G_{11}^*	G_{12}^*	G_{44}^*	$G_{44}'^*$
−0.24	2.5	0.49	1.2	−7.0	0.05	−0.015	0.038	7.9×10^{-4}	-2.5×10^{-4}	8.9×10^{-4}	2	0.0	1	1

$$G_{11}^* = G_{11}/G_{110}, \quad G_{12}^* = G_{12}/G_{110}, \quad G_{44}^* = G_{44}/G_{110}, \quad G_{44}'^* = G_{44}'/G_{110}, \tag{9}$$

where P_0 is the magnitude of the spontaneous polarization at room temperature, G_{110} is a reference value of the gradient energy coefficients, and α_0 represents the value of α_1 at 25 °C. The superscript asterisk, *, denotes the dimensionless value of the corresponding variable.

With the dimensionless variables and ignoring the surface energy term, we explicitly express the 2D time-dependent Ginzburg-Landau equation as follows:

$$\frac{\partial P_1^*}{\partial t^*} = -\Big[2\alpha_1^* P_1^* + 4\alpha_{11}^* P_1^{*3} + 2\alpha_{12}^* P_1^* P_2^{*2} + 6\alpha_{111}^* P_1^{*5} + \alpha_{112}^*(4P_1^{*3}P_2^{*2} + 2P_1^* P_2^{*4}) - 2Q_{11}^*\sigma_{11}P_1^* - 2Q_{12}^*\sigma_{22}P_1^* - Q_{44}^*\sigma_{12}P_2^* - G_{11}^* P_{1,xx}^* - (G_{12}^* + G_{44}^* - G_{44}'^*)P_{2,xy}^* - (G_{44}^* + G_{44}'^*)P_{1,yy}^* - \tfrac{1}{2}E_1^{d^*} - E_1^{a^*}\Big], \tag{10a}$$

$$\frac{\partial P_2^*}{\partial t^*} = -\Big[2\alpha_1^* P_2^* + 4\alpha_{11}^* P_2^{*3} + 2\alpha_{12}^* P_2^* P_1^{*2} + 6\alpha_{111}^* P_2^{*5} + \alpha_{112}^*(4P_2^{*3}P_1^{*2} + 2P_2^* P_1^{*4}) - 2Q_{11}^*\sigma_{22}P_2^* - 2Q_{12}^*\sigma_{11}P_2^* - Q_{44}^*\sigma_{12}P_1^* - G_{11}^* P_{2,yy}^* - (G_{12}^* + G_{44}^* - G_{44}'^*)P_{1,xy}^* - (G_{44}^* + G_{44}'^*)P_{2,xx}^* - \tfrac{1}{2}E_2^{d^*} - E_2^{a^*}\Big]. \tag{10b}$$

The finite difference method for spatial derivatives and the Runge-Kutta method of order four for temporal derivatives are employed to solve Eq. (10) in real space with the zero boundary condition. At the beginning of the evolution, a Gaussian random fluctuation is introduced to initiate the spontaneous polarization evolution process.

C. Boundary conditions for static electrical and mechanical equilibrium equations

The electrical and mechanical boundary conditions have a significant effect on the equilibrium domain structures and spontaneous polarization instability. To obtain the electrostatic potential from Eq. (5), the boundary condition of the electrostatic potential should be specified. For a simulated ferroelectroic island, we set the electrostatic potential $\phi=0$ at the three free surfaces and the interface between the island and the substrate, as shown in Fig. 1(a), which is called the short circuit condition. For a simulated thin film without any applied field, the periodic boundary condition for the electrostatic potential is adopted in the x_2 direction and the electrostatic potential is set at zero, i.e., $\phi=0$, at the top free surface and the interface between the film and the substrate, as shown in Fig. 1(b). When an external field, E_1^a, is applied along the thickness direction of thin films, the electrostatic potential is zero at the surface and $-E_1^a d$ at the interface between the film and the substrate ($E_1^d = -\phi,_1 - E_1^a$ in this case). With the electric boundary condition, Eq. (5) is numerically solved by using the finite difference method.

A spontaneous polarization field in a ferroelectric island or film can induce inhomogeneous elastic fields in both the ferroelectric material and the substrate due to the constraint of the substrate. The mechanical boundary conditions for a ferroelectric island are taken as: the three free surfaces are traction-free and the interface between the island and the substrate is mechanically coherent, which means the traction continuity and the displacement continuity. At the paraelectric state, the entire system including the simulated ferroelectric material and the substrate is treated to be stress-free, indicating no lattice mismatch between the island or film and the substrate at the paraelectric phase. The elastic deformation of the substrate is calculated only in the area surrounded by the dotted lines, as shown in Fig. 1, meaning that the deformation of the substrate outside the dotted lines should be ignorable. For a thin film, the traction-free and the coherent boundary conditions are applied along the free surface and the interface, respectively, and the periodic boundary condition is used along the x_2 direction. With these boundary conditions, we employ the finite element method to solve the mechanical governing equation for a given spontaneous polarization field (see the Appendix for details).

D. Parameters used in the simulations

The material parameters of $PbTiO_3$ are taken as an example in the present simulations. We set the magnitude of the spontaneous polarization at room temperature to be $P_0 = |\mathbf{P}_0| = 0.757\ \mathrm{C/m^2}$, the reference value of the gradient energy coefficients as $G_{110} = 1.73\times10^{-10}\ \mathrm{m^4N/C^2}$, the relative dielectric constant, $\kappa = 66.0$, and the value of α_1 at 25 °C to be $\alpha_0 = \alpha_{1,25\,^\circ\mathrm{C}} = (T - T_0)/(2\varepsilon_0 C_0) = (25-479)\times3.8\times10^5\ \mathrm{m^2N/C^2}$, where T is in units of °C. The values of the dimensionless (normalized) material coefficients used in the simulations are listed in Table I.

In the simulations, we use N1 × N2 discrete grids for a ferroelectric material with a cell size of $\Delta x_1^* = \Delta x_2^* = \Delta l^*$. The different length-to-thickness ratios and different sizes of the ferroelectrics can be realized by giving different numbers to N1 and N2, and/or by giving different unit lengths to Δl^*. The domain structure is represented by the spontaneous polarization field, in which spontaneous polarizations vary spatially and each spontaneous polarization is characterized by a two-component vector in the 2D simulations, i.e., by an electric dipole. The length and direction of the electric dipole denote the magnitude and direction of local polarization, respectively. The rectangular element size in the finite element calculations is also set as $\Delta x_1^* = \Delta x_2^* = \Delta l^*$ for both ferroelectric material and substrate.

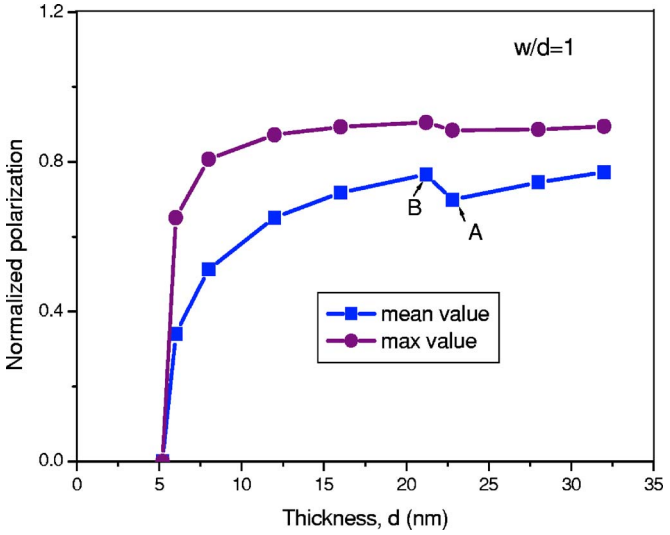

FIG. 2. (Color online) The dependence of dipole magnitude on the ferroelectric island size ($w/d=1$).

III. SIMULATION RESULTS AND DISCUSSION

A. Size effect in epitaxial islands with $w=d$

For a 2D ferroelectric epitaxial island with the same size in thickness and length, i.e., $w=d$, as shown in Fig. 1(a), the discrete grids are N1=N2=40 in both thickness and length directions, and the grid length Δl^* changes from 0.8 to 0.13, which corresponds a real grid length Δl ranging from 0.8 nm to 0.13 nm. The time step is set at $\Delta t^*=0.004$ and total number of steps is 8000 in solving Eq. (10), which ensures that the domain structure reaches its steady state.[15]

Figure 2 shows that the mean magnitude and the maximum magnitude of polarizations as functions of the ferroelectric size. The mean magnitude of the polarization, $\langle P_s^* \rangle$, is obtained by averaging the dipole magnitude, $P_s^* = \sqrt{P_1^{*2}+P_2^{*2}}$, at each grid over the entire simulated ferroelectric material. Figure 2 indicates that both mean magnitude and maximum magnitude approach zero as the island size is reduced to 5.2 nm, thereby showing that spontaneous polarizations disappear when the island size is equal to or smaller than 5.2 nm. Since the δ value plays a crucial role in the estimation of the critical size for the disappearance of polarizations, we will not pay too much attention to the critical size because of the uncertainness of the δ value used by different researchers. Figure 2 shows also a sudden increase in the mean (or maximum) magnitude curve when the island size is reduced from 22 nm to 21 nm. The sudden increase is caused by the change from a multidomain state to a monodomain state in the simulated island, as evidenced by the domain structures shown in Figs. 3(a) and 3(b) for the island sizes of 22 nm and 21 nm, respectively, where one of every two dipoles is plotted for clarity. When $w=d=22$ nm, the ferroelectric island forms a two-domain structure with a 180° domain wall, as shown in Fig. 3(a). The formation of a 180° domain wall rather than a 90° domain wall indicates that the electrostatic interaction is predominant in this case in comparison with the elastic interaction. The directions of the dipoles in the two domains are parallel or antiparallel to the x_1 direction due to no mechanical constraint along the x_1 direction. The dipole magnitude inside the domains is much larger than that near the domain wall. The two-domain structure changes to a monodomain structure when the island size decreases from 22 nm to 21 nm, and the change in the domain structure induces the sudden increase in both mean and maximum magnitudes because of the elimination of the 180° domain wall. After that, further decreasing the island size reduces both magnitudes of spontaneous polarizations, as shown in Fig. 2. Eventually, both magnitudes of polarizations approach zero in a second phase transformation manner. Experimentally, Jiang *et al.* observed that the $PbTiO_3$ particles are in the monodomain structure when the particle size is less than 20 nm.[4] The critical size, for the transition from the multidomain state to the monodomain state, determined from the phase field simulation is consistent with the experimental result.

B. Size effect in epitaxial islands with $w=2d$

Ferroelectric 2D islands with length being twice the thickness, i.e., $w=2d$, are simulated to study the lateral size effect on domain structures. The discrete grids are taken as N1=30 and N2=60 in thickness and length directions, respectively. The grid length Δl^* changes from 0.13 to 0.7, corresponding to a real length ranging from 0.13 nm to 0.7 nm. Figure 4 shows the mean magnitude and the maximum magnitude of polarizations as functions of the island thickness. The critical size for the transition from a multidomain state to a monodomain state and the critical size for the disappear-

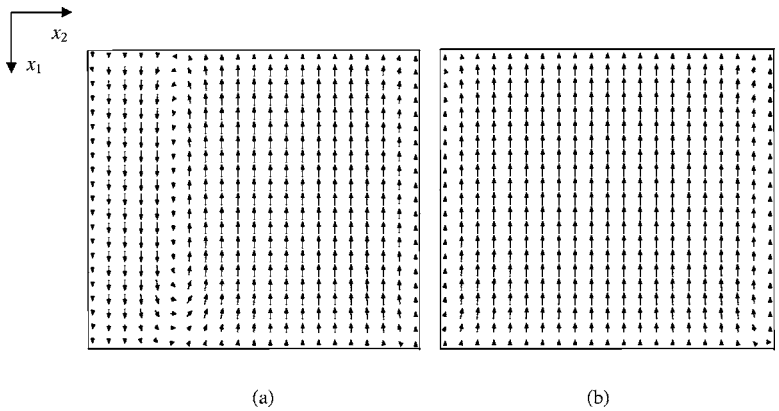

FIG. 3. Domain structures with island sizes of (a) 22 nm and (b) 21 nm, which correspond to points A and B in Fig. 2, respectively.

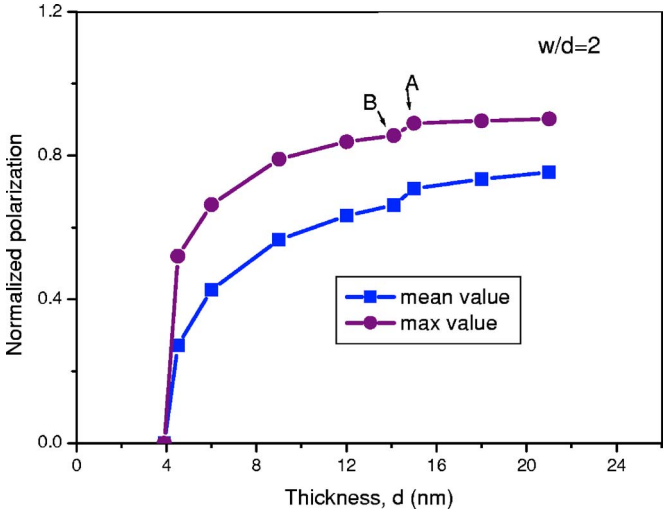

FIG. 4. (Color online) The dependence of dipole magnitude on the thickness of ferroelectric islands of $w/d=2$.

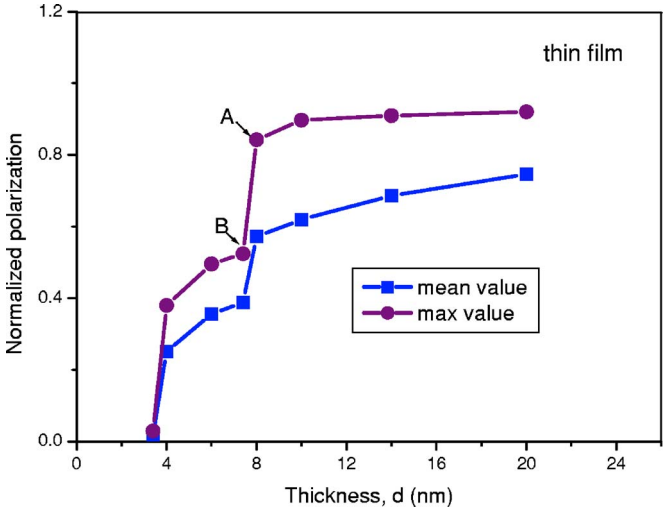

FIG. 6. (Color online) The dependence of dipole magnitude on the film thickness.

ance of polarizations are found to be 15 nm and 3.9 nm, respectively. Figures 5(a) and 5(b) show the ferroelectric domain structures for the island thicknesses of $d=15$ nm and 14.1 nm, respectively, where again, one of every two dipoles is plotted for clarity. When $d=15$ nm, the polarizations form a two-domain structure with a 90° domain wall, as shown as Fig. 5(a), and the corresponding mean and maximum magnitudes of polarizations are marked by A in Fig. 4. The formation of the 90° domain wall indicates that the elastic interaction is predominant in this case in comparison with the electrostatic interaction. Figure 5(a) shows that dipoles in one domain are antiparallel to the x_1 direction and dipoles in another domain are parallel to the x_2 direction. The dipoles parallel to the x_2 direction are subjected to more mechanical

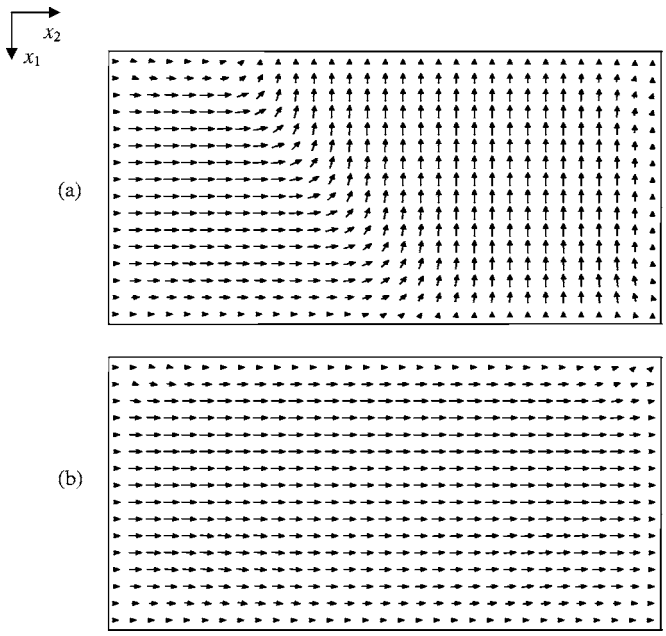

FIG. 5. Domain structures with different thickness (a) 15 nm and (b) 14.1 nm, which correspond to points A and B in Fig. 4, respectively.

constraint from the substrate than the dipoles antiparallel to the x_1 direction. In general, a tensile or compressive stress along the dipole direction can enhance or reduce the magnitude of the dipole. Therefore, the average magnitude of the dipoles parallel to the x_2 direction is smaller than that of the dipoles antiparallel to the x_1 direction. When the island thickness is reduced to 14.1 nm, a monodomain structure occurs with all dipoles parallel to the x_2 direction, as shown in Fig. 5(b). The corresponding mean and maximum magnitudes of polarizations are suddenly decreased from point A to point B in Fig. 4 due to the elimination of the 90° domain wall and the switch of the dipoles antiparallel to the x_1 direction to parallel to the x_2 direction. After this critical thickness, both magnitudes of polarizations decrease as the island thickness is reduced, as shown in Fig. 4, and eventually to zero at the thickness of 3.9 nm. The critical size for the transition from the multidomain state to the monodomain state in the case of $w/d=2$ are much smaller than that in the case of $w/d=1$, thereby illustrating that the length-to-thickness ratio has a significant influence on the domain instability in epitaxial ferroelectric islands.

C. Size effect in epitaxial thin films

A thin film can be regarded to have an infinitely large value of the length-to-thickness ratio. In the present study of ferroelectric thin films, the discrete grids are taken as N1 $=20$ and N2$=80$ in the thickness direction and along the film direction, respectively. The dimensionless unit length, Δl^*, changes from 0.17 to 1, corresponding to a real length ranging from 0.17 nm to 1 nm. Figure 6 shows that the mean magnitude and the maximum magnitude of polarizations as functions of the film thickness. The critical size for the transition from a multidomain state to a monodomain state and the critical size for the disappearance of polarizations are found to be 8 nm and 3.4 nm, respectively. Figures 7(a) and 7(b) show the ferroelectric domain structures for the film thicknesses of $d=8$ nm and 7.4 nm, respectively, where again, one of every two dipoles is plotted for clarity. For the

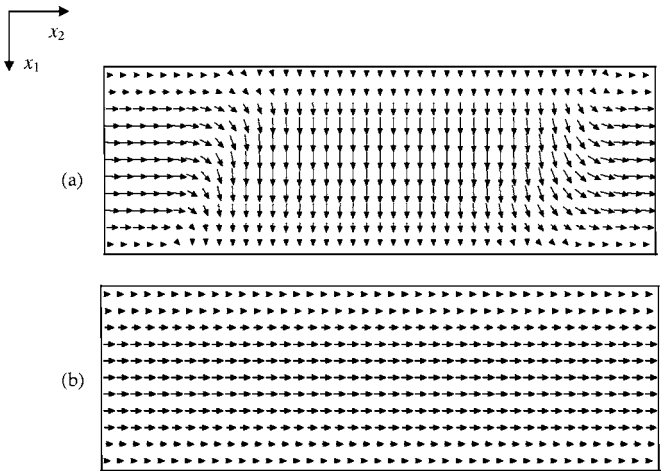

FIG. 7. Domain structures for the thicknesses of (a) 8 nm and (b) 7.4 nm, which correspond to points A and B in Fig. 6, respectively.

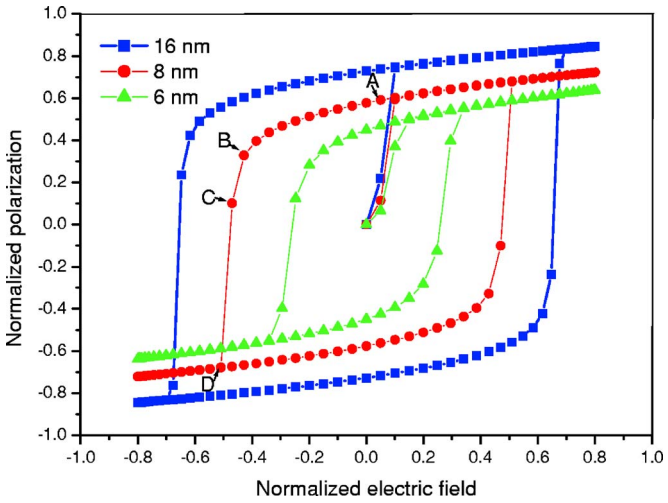

FIG. 8. (Color online) Hysteresis loops in ferroelectric thin films with thicknesses of 6, 8, and 16 nm.

film with a thickness of $d=8$ nm, the polarizations form an $a/c/a$ type multidomain structure with 90° domain walls between a and c domains, in which the dipoles are parallel to the x_2 and x_1 directions, respectively, and the corresponding magnitudes are marked by A in Fig. 6. The main driving force for the formation of the $a/c/a$ multidomain structure is the reduction of the elastic energy in the thin film. For the film with a thickness of 7.4 nm, the polarizations appear in a single domain with all dipoles parallel to the x_2 direction, as shown in Fig. 7(b), which gives the polarization magnitudes marked by B in Fig. 6. Comparing Fig. 6 with Fig. 4 indicates that the sudden decrease in both mean magnitude and maximum magnitude of polarizations is more significant when the length-to-thickness ratio increases from two to infinity due to a more mechanical constraint from the substrate. Further reducing the film thickness, the monodomain structure remains unchanged, but the polarization magnitudes decrease because of the intrinsic edge effect related to the extrapolation length. The appearance of the monodomain structure rather than a multidomain structure in thin films indicates that a thin film/substrate system can tolerate a large mismatch strain induced by polarizations as long as the film is thinner than a critical thickness. Both critical sizes for the transition from the multidomain state to the monodomain state and for the disappearance of polarizations in the case of thin films are smaller than those in both cases of islands. This is because the lateral constraint is the strongest in thin films.

D. Size effect of polarization switching in epitaxial thin films

It is polarization switching that causes ferroelectric materials to exhibit ferroelectric and nonlinear dielectric behaviors. In order to characterize the ferroelectric and nonlinear dielectric behaviors of ferroelectric epitaxial thin films, we simulate the polarization response of a thin film under an external electric loading with a sine form at room temperature, 25 °C. The external electric field E_1^{a*} is applied along the thickness direction, i.e., the x_1 axis, where a positive or negative electric field means that the field is parallel or antiparallel to the x_1 direction. At each iteration step i, the applied electric field changes as sine function: $E_1^{a*}=0.8\sin(2\pi i/50\,000)$. When i increases from zero to 12 500, 25 000, 37 500, 50 000, and 62 500, the electric field E_1^{a*} changes from zero to 0.8, 0.0, −0.8, 0.0, and 0.8. At each applied electric field, the simulated ferroelectric film is allowed to evolve one step with the step time of $\Delta t^*=0.004$, which corresponds a loading frequency of 0.005. The average polarization along the x_1 direction is taken as the macroscopic response of the simulated ferroelectric thin film.

Figure 8 shows simulated results of the average polarization $\langle P_1^* \rangle$ versus the electric field E_1^{a*} for ferroelectric thin films with thicknesses of 6 nm, 8 nm, and 16 nm. Under the applied electric field, the polarizations in each of the films are all parallel or/and antiparallel to the electric field. Taking the 8 nm thick film as an example, we plot the polarization distributions in the thin film at the electric fields of 0, −4.3, −4.7, and −5.1 in Figs. 9(a)–9(d), respectively, which correspond to points A–D in Fig. 8. When the applied field is reduced to zero from a highly positive value of 0.8, the polarization distribution is in a single domain, as shown in Fig. 9(a), where the magnitudes of dipoles in the middle region is much higher than in the regions near the surface and the interface, which is caused by the used zero boundary condition. When the applied negative field increases its magnitude to −4.3, the average polarization reduces its magnitude, but the polarization pattern remains unchanged, as shown in Fig. 9(b). After this, when the applied negative field increases its magnitude to −4.7, polarization switching takes place by nucleate new domains at the surface and the interface of the thin film, as illustrated in Fig. 9(c). In the 2D simulations, the new domains are homogeneously nucleated along the surface and the interface because in these regions, the polarization magnitude is small such that the energy barrier for the polarizations to switch 180° must be low. After the nucleation of new domains, the new domains will grow by domain wall motion. When the applied field increases its magnitude to −5.1, the macroscopic polarization switching is completed

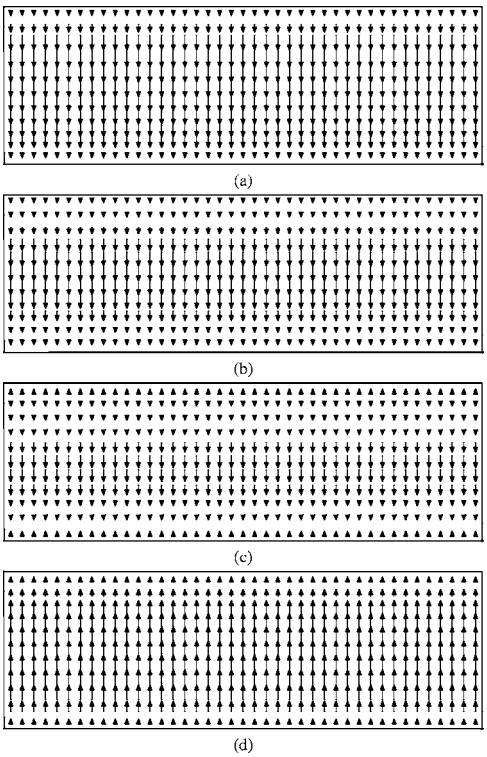

FIG. 9. The polarization distribution of the 8 nm thick film under applied electric fields of (a) 0, (b) −4.3, (c) −4.7, and (d) −5.1, which correspond to points A, B, C, and D in Fig. 8, respectively.

and a single domain is formed. Comparing Figs. 9(d) with 9(a) indicates that the two single domain structures are similar except of the 180° switching in the polarizations.

Figure 8 shows that the smaller the film thickness is, the smaller the hysterisis loop of the average polarization versus the electric field will be. Each hysteresis loop gives a remanent polarization, P_r^*, which is defined as the average polarization along the applied field direction when the applied field is reduced to zero from its high magnitude, and a coercive field, which is defined as the critical value of the applied field, at which macroscopic polarization switch occurs. Clearly, both the remanent polarization and coercive field decrease their magnitudes as the film thickness is reduced.

The remanent polarization can be predicted from thermodynamics. In the thermodynamic calculations,[27] the free energy of a thin film with spatially inhomogeneous polarizations is expressed in terms of renormalized coefficients a, b, and c as $\bar{F}=a\langle P\rangle^2+b\langle P\rangle^4+c\langle P\rangle^6$, where $\langle P\rangle$ denotes the average polarization in the thin film. The renormalized coefficients, a, b, and c, depend on temperature, film thickness, the extrapolation length, and the gradient coefficients.[28] The remanent polarization in the thin film is calculated from the free energy and given by $\langle P\rangle^2=[-b+(b^2-3ac)^{1/2}]/3c$. Using the same material constants as used in the simulations, we calculate the remanent polarizations and plot them with a solid line in Fig. 10. For comparison, the remanent polarizations determined from the phase field simulations are also illustrated with square points in Fig. 10. Figure 10 shows that the remanent polarization obtained from the phase field simulations is more or less the same as that obtained from

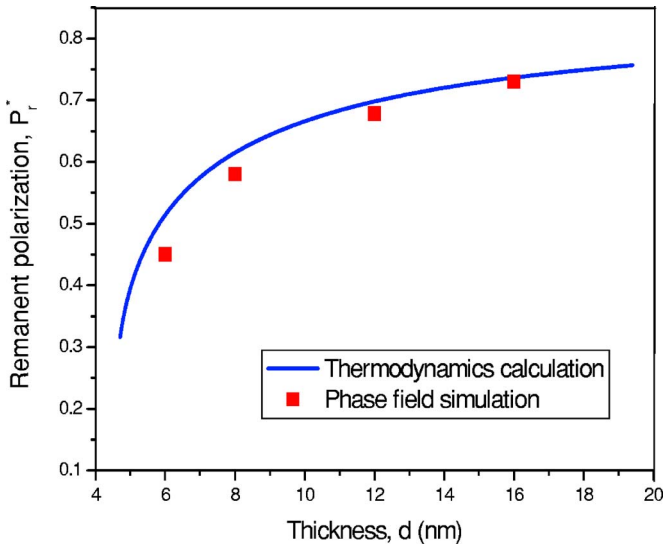

FIG. 10. (Color online) The remanent polarization versus the film thickness. The solid line is obtained from the thermodynamic calculations[24] and the square points are obtained from the present phase field simulations.

the thermodynamic calculation. The inconsistency between the two predictions may be attributed to the lack of the long-range elastic interaction in the thermodynamic calculation. Nevertheless, the decrease of remanent polarization with decreasing film thickness has been observed in recent experiments on ultrathin ferroelectric $BaTiO_3$ films,[29] which is in agreement with the theoretical predictions.

IV. CONCLUDING REMARKS

In summary, the present phase field simulations exhibit two size-dependent behaviors. The first critical size is for the transition from a multidomain structure to a monodomain structure and the second critical size is for the disappearance of spontaneous polarizations. Both critical sizes will be small if the laterally mechanical constraint is strong, i.e., if the length-to-thickness ratio is large. For the simulated perfect ferroelectric films without other defects, macroscopic polarization switching is through nucleation of new domains at the surface and the interface and domain wall motion (new domains grow and the parent domain shrinks). The remanent polarization and the coercive field both decrease as the film thickness is reduced. If the long-range electrostatic interaction is dominated in comparison to the long-range elastic interaction, a 180° domain wall will be formed, which occurs in the epitaxial ferroelectric inlands of length equaling thickness. On the other hand, if the long-range elastic interaction is dominated in comparison to the long-range electrostatic interaction, a 90° domain wall(s) will be formed, which occurs in the epitaxial ferroelectric inlands with length-to-thickness being equal to or larger than two. The present simulation results are consistent with the experimental observations[30] that $PbTiO_3$ grains in a dense film contain laminar 90° domain walls, whereas separated $PbTiO_3$ grains have mainly 180° domain walls.

It should be noted that the present work is based on the Landau-Ginzburg thermodynamic theory. The critical size for the disappearance of spontaneous polarizations is strongly dependent on the boundary condition of spontaneous polarizations adopted in the simulations. As mentioned above, the present study does not discuss the absolute value of the critical size for the disappearance of spontaneous polarizations. In addition, the present simulations do not consider any defects. When defects are present, new domains are usually nucleated from the defects and this type of nucleation is called heterogeneous nucleation, which is different from the homogeneous nucleation observed in the simulations. Heterogeneous nucleation generally leads to a much lower coercive field. Therefore, the thickness-dependent coercive field observed in the present simulations represents the intrinsic coercive field, which scales linearly with the polarizations.[31] In real ferroelectric thin films there exist defects and the number of defects is, in general, increased with the film thickness. That is why the coercive field observed in experiments could be lower when the film is thicker.[32]

ACKNOWLEDGMENTS

This work was fully supported by an RGC grant from the Research Grants Council of the Hong Kong Special Administrative Region, China.

APPENDIX

For materials with the perovskite crystal structure, the phase transition from paraelectric phase to ferroelectric phase changes the crystal system from cubic to tetragonal and generates spontaneous polarizations and spontaneous strains. The spontaneous strains at a stress-free state, which are called eigenstrains, are associated with the spontaneous polarizations in the following form (Ref. 22):

$$\begin{aligned}
\varepsilon_{11}^0 &= Q_{11}P_1^2 + Q_{12}(P_2^2 + P_3^2),\\
\varepsilon_{22}^0 &= Q_{11}P_2^2 + Q_{12}(P_3^2 + P_1^2),\\
\varepsilon_{33}^0 &= Q_{11}P_3^2 + Q_{12}(P_1^2 + P_2^2),\\
\varepsilon_{23}^0 &= Q_{44}P_2P_3,\\
\varepsilon_{13}^0 &= Q_{44}P_1P_3,\\
\varepsilon_{12}^0 &= Q_{44}P_1P_2,
\end{aligned} \tag{A1}$$

where Q_{11}, Q_{12}, and Q_{44} are the electrostrictive coefficients. Elastic strains are usually generated in a ferroelectric material, which are calculated by

$$e_{ij} = \varepsilon_{ij} - \varepsilon_{ij}^0, \tag{A2}$$

where ε_{ij} are total strains, which must be compatible and are defined by

$$\varepsilon_{ij} = \frac{1}{2}(u_{i,j} + u_{j,i}), \tag{A3}$$

in which u_i are displacements. In linear elasticity, stresses, σ_{ij}, are related to elastic strains through Hooke's law:

$$\sigma_{ij} = c_{ijkl}e_{kl} = c_{ijkl}(\varepsilon_{ij} - \varepsilon_{ij}^0). \tag{A4}$$

Without any body forces, the mechanical equilibrium equations are expressed as follows:

$$\sigma_{ij,j} = 0. \tag{A5}$$

With the periodic boundary condition, Eq. (A5) can be solved in Fourier space analytically. However, it is impossible to solve Eq. (A5) analytically in real space for a finite-size ferroelectric material with arbitrary boundary conditions. Instead the finite element method is used to solve Eq. (A5) numerically. Using the variation relationship, Eq. (A5) is changed into

$$\int_V \sigma_{ij}\delta\varepsilon_{ij}dV = \int_S t_k\delta u_k dS, \tag{A6}$$

where $t_k = n_i\sigma_{ik}$ are tractions on the surface.

For simplicity, the substrate is assumed to have the same elastic properties as the ferroelectric material. Thus, letting polarizations be zeros allows Eq. (A4) to be applied to the substrate. For 2D calculations, (A4) can be rewritten in matrix form as

$$\{\sigma\} = [C]\{\varepsilon\} - [C][Q]\{P\}, \tag{A7}$$

where

$$\{\sigma\} = \begin{Bmatrix}\sigma_{11}\\ \sigma_{22}\\ \sigma_{12}\end{Bmatrix}, \quad \{\varepsilon\} = \begin{Bmatrix}\varepsilon_{11}\\ \varepsilon_{22}\\ 2\varepsilon_{12}\end{Bmatrix}, \quad \{P\} = \begin{Bmatrix}P_1^2\\ P_2^2\\ P_1\ P_2\end{Bmatrix},$$

$$[C] = \begin{bmatrix}c_{11} & c_{12} & 0\\ c_{12} & c_{11} & 0\\ 0 & 0 & c_{44}\end{bmatrix}, \quad \text{and } [Q] = \begin{bmatrix}Q_{11} & Q_{12} & 0\\ Q_{12} & Q_{11} & 0\\ 0 & 0 & Q_{44}\end{bmatrix}. \tag{A8}$$

Four-node plane square elements are employed to the discrete simulated structure. Letting $\delta_i = [u_i\ v_i]$ $(i = 1,2,3,4)$, in which u_i and v_i denote the displacement of ith node in the x_1 and x_2 directions, respectively, the displacement vector of the four nodes in each element is expressed by

$$\{\delta^e\} = [\delta_1\ \delta_2\ \delta_3\ \delta_4]^T. \tag{A9}$$

The displacements in the element are expressed in terms of the node displacements:

$$u = \sum_{i=1}^{4} N_{ui}u_i \quad \text{and} \quad v = \sum_{i=1}^{4} N_{vi}v_i, \tag{A10}$$

where N_{ui} and N_{vi} are the interpolation functions. Equation (A10) can be rewritten in matrix form as

$$\begin{Bmatrix}u\\ v\end{Bmatrix} = [N_1\ N_2\ N_3\ N_4]\begin{Bmatrix}\delta_1^T\\ \delta_2^T\\ \delta_3^T\\ \delta_4^T\end{Bmatrix} = [N]\{\delta^e\}, \tag{A11}$$

in which

$$N_i = \begin{bmatrix} N_{ui} & \\ & N_{vi} \end{bmatrix}. \tag{A12}$$

The strain of the element can then be obtained from the displacements as

$$\{\varepsilon\} = [L]\begin{Bmatrix} u \\ v \end{Bmatrix} = [L][N]\{\delta^e\} = [B]\{\delta^e\}, \tag{A13}$$

where

$$[L] = \begin{bmatrix} \frac{\partial}{\partial x} & 0 \\ 0 & \frac{\partial}{\partial y} \\ \frac{\partial}{\partial y} & \frac{\partial}{\partial x} \end{bmatrix} \quad \text{and} \quad [B] = [L][N].$$

Because the surface is traction-free, i.e., $t_k=0$, and the substrate boundary denoted by dot lines is fixed, i.e., $\delta u_k=0$, Eq. (A6) is reduced to

$$\begin{aligned} \int\int_A \{\sigma\}^T \delta\{\varepsilon\} dA &= \int\int_A ([C]\{\varepsilon\} - [C][Q]\{P\})^T \delta\{\varepsilon\} dA \\ &= \int\int_A ([C][B]\{\delta^e\} \\ &\quad - [C][Q]\{P\})^T B\,\delta\{\delta^e\} dA = 0. \end{aligned} \tag{A14}$$

Based on the variation principle, the following element equation can be obtained:

$$[K^e]\{\delta^e\} = \{F^e\}, \tag{A15}$$

where

$$[K^e] = \int\int_{A_e} B^T[C]B dA \quad \text{and} \quad \{F^e\} = \int\int_{A_e} B^T[C][Q] \times \{P\} dA \tag{A16}$$

are the element stiffness matrix and element node force vector, respectively. Assembling all the stiffness matrix, displacement vector, and force vector of the elements together yields the globe equation:

$$KU = F, \tag{A17}$$

where

$$K = \sum_e [K^e] \quad \text{and} \quad F = \sum_e \{F^e\} \tag{A18}$$

are the globe stiffness matrix and the node force matrix, respectively, and U is the vector containing all node displacements. The node displacements are obtained by solving the linear array Eq. (A17), with the LAPACK routines for a symmetric positive definite banded system.

*Corresponding author. Email address: mezhangt@ust.hk

[1] T. M. Shaw, S. Trolier-McKinstry, and P. C. McIntyre, Annu. Rev. Mater. Sci. **30**, 263 (2000).
[2] C. H. Ahn, K. M. Rabe, and J. M. Triscone, Science **303**, 488 (2004).
[3] M. G. Stachiotti, Appl. Phys. Lett. **84**, 251 (2004).
[4] B. Jiang, J. L. Peng, L. A. Bursill, and W. L. Zhong, J. Appl. Phys. **87**, 3462 (2000).
[5] W. L. Zhong, Y. G. Wang, P. L. Zhang, and B. D. Qu, Phys. Rev. B **50**, 698 (1994).
[6] H. Fu and L. Bellaiche, Phys. Rev. Lett. **91**, 257601 (2003).
[7] I. Kornev, H. Fu, and L. Bellaiche, Phys. Rev. Lett. **93**, 196104 (2004).
[8] J. Junquera and P. Ghosez, Nature (London) **422**, 506 (2003).
[9] I. I. Naumov, L. Bellaiche, and H. Fu, Nature (London) **432**, 737 (2004).
[10] S. Tinte, M. G. Stachiotti, M. Sepliarsky, R. L. Migoni, and C. O. Rodriguez, J. Phys.: Condens. Matter **11**, 9679 (1999).
[11] Y. G. Wang, W. L. Zhong, and P. L. Zhang, Phys. Rev. B **51**, 5311 (1995).
[12] S. Li, J. A. Eastman, Z. Li, C. M. Foster, R. E. Newnham, and L. E. Cross, Phys. Lett. A **212**, 341 (1996).
[13] O. G. Vendik and S. P. Zubko, J. Appl. Phys. **88**, 5343 (2000).
[14] J. Wang, S. Q. Shi, L. Q. Chen, Y. L. Li, and T. Y. Zhang, Acta Mater. **52**, 749 (2004).
[15] J. Wang, Y. L. Li, L. Q. Chen, and T. Y. Zhang, Acta Mater. **53**, 2495 (2005).
[16] R. Ahluwalia and W. Cao, J. Appl. Phys. **93**, 537 (2003).
[17] Y. L. Li, S. Y. Hu, Z. K. Liu, and L. Q. Chen, Acta Mater. **50**, 395 (2002).
[18] S. Nambu and D. A. Sagala, Phys. Rev. B **50**, 5838 (1994).
[19] H. L. Hu and L. Q. Chen, J. Am. Ceram. Soc. **81**, 492 (1998).
[20] W. Cao, S. Tavener, and S. Xie, J. Appl. Phys. **86**, 5739 (1999).
[21] W. Zhang and K. Bhattacharya, Acta Mater. **53**, 185 (2005).
[22] M. E. Lines and A. M. Glass, *Principles and Applications of Ferroelectrics and Related Materials*, (Clarendon, Oxford, 1977).
[23] M. J. Haun, E. Furman, S. J. Jang, H. A. McKinstry, and L. E. Closs, J. Appl. Phys. **62**, 3331 (1987).
[24] R. Kretschmer and K. Binder, Phys. Rev. B **20**, 1065 (1979).
[25] Y. L. Li, S. Y. Hu, Z. K. Liu, and L. Q. Chen, Appl. Phys. Lett. **81**, 427 (2002).
[26] W. Kanzig, Phys. Rev. **98**, 549 (1955).
[27] M. D. Glinchuk, E. A. Eliseev, and V. A. Stephanovich, J. Appl. Phys. **93**, 1150 (2003).

[28]

$$a = \frac{\alpha_1(1 - A_1/f)}{1 - A_1}, \quad b = \frac{\alpha_{11}(1 - A_2)}{(1 - A_1)^4}, \quad c = \frac{\alpha_{111}(1 - A_3)}{(1 - A_1)^6},$$

$$\text{in which } A_1 = \frac{2U}{h}, \quad f = -\alpha_1/(2\pi),$$

$$A_2 = \frac{48U - 36U^2 + 16U^3 - 3U^4}{6h},$$

$$A_3 = \frac{360U - 450U^2 + 400U^3 - 225U^4 + 72U^5 - 10U^6}{30h},$$

$$U = 1/(1 + \delta\sqrt{4\pi(1 - f)/G_{11}}), \quad h = d\sqrt{4\pi(1 - f)/G_{11}}.$$

[29] Y. S. Kim, D. H. Kim, J. D. Kim, Y. J. Chang *et al.*, Appl. Phys. Lett. **86**, 102907 (2005).

[30] A. Roelofs, T. Schneller, K. Szot, and R. Waser, Appl. Phys. Lett. **81**, 5231 (2002).

[31] V. M. Fridkin and S. Ducharme, Phys. Solid State **43**, 1268 (2001).

[32] V. Nagarajan, S. Prasertchoung, T. Zhao, H. Zheng, J. Ouyang, R. Ramesh, W. Tian, X. Q. Pan, D. M. Kim, C. B. Eom, H. Kohlstedt, and R. Waser, Appl. Phys. Lett. **84**, 5225 (2004).